

Multiscale Representation for Real-Time Anti-Aliasing Neural Rendering

Dongting Hu
University of Melbourne

Zhenkai Zhang
University of Melbourne

Tingbo Hou
Google

Tongliang Liu
University of Sydney

Huan Fu*
Alibaba Group

Mingming Gong*
University of Melbourne

Abstract

The rendering scheme in neural radiance field (NeRF) is effective in rendering a pixel by casting a ray into the scene. However, NeRF yields blurred rendering results when the training images are captured at non-uniform scales, and produces aliasing artifacts if the test images are taken in distant views. To address this issue, Mip-NeRF proposes a multiscale representation as a conical frustum to encode scale information. Nevertheless, this approach is only suitable for offline rendering since it relies on integrated positional encoding (IPE) to query a multilayer perceptron (MLP). To overcome this limitation, we propose mip voxel grids (Mip-VoG), an explicit multiscale representation with a deferred architecture for real-time anti-aliasing rendering. Our approach includes a density Mip-VoG for scene geometry and a feature Mip-VoG with a small MLP for view-dependent color. Mip-VoG encodes scene scale using the level of detail (LOD) derived from ray differentials and uses quadrilinear interpolation to map a queried 3D location to its features and density from two neighboring downsampled voxel grids. To our knowledge, our approach is the first to offer multiscale training and real-time anti-aliasing rendering simultaneously. We conducted experiments on multiscale datasets, and the results show that our approach outperforms state-of-the-art real-time rendering baselines.

1. Introduction

Novel view synthesis is an appealing and challenging problem in the field of computer vision and graphics. Recently, neural volumetric representations such as neural radiance field (NeRF) [33] have achieved great success in reconstructing 3D scenes from a set of multi-view images. NeRF uses a coordinate-based multilayer perceptron (MLP)

Method	Multiscale Training	Real-time Rendering	Anti-aliasing Rendering
Mip-NeRF [3]	✓		✓
SNeRG [19]		✓	
MobileNeRF [9]		✓	✓
Ours	✓	✓	✓

Table 1: Our method is the first one concurrently addresses multiscale training, real-time rendering, and anti-aliasing rendering.

to map a 5D input coordinate (3D position and 2D viewing direction) to the properties of the scene (volume density and view-dependent emitted radiance) at that location. To render a pixel, NeRF casts a ray through the pixel into the scene, queries the scene representation for the sampled points along that ray, and composites the final color. Such rendering procedure performs well if the training and test images exhibit the uniform resolution. Given the training images with multiple resolution, NeRF would yield excessively blurred rendering results, due to the variation of the pixel’s footprint from different scales. Besides, in case that testing views are far from the distance of the training images, the sample rate for per pixel would be inadequacy, resulting in aliasing artifacts.

To efficiently tackle this issue, Mip-NeRF [3] presents a continuously-valued scale representation for coordinate-based models. Mip-NeRF introduces an integrated positional encoding (IPE) method to represent a sub-region against a single point and renders the conical frustums instead of rays. Mip-NeRF successfully performs the multiscale training and effectively alleviates the aliasing artifacts. However, since this approach relies on querying the network with the scale-variant IPE, it cannot be extended to real-time rendering paradigms by using the pre-cache techniques [19].

In this paper, we propose a multiscale representation, namely mip (multum in parvo, as in “mipmap”) voxel grids

*Equal contribution

(Mip-VoG), that enables training from images with different scales, and enjoys efficient anti-aliasing rendering at the inference stage. We first introduce a “deferred” NeRF variant that explicitly stores the scene geometry and color properties in Mip-VoG, and encodes view-dependent effects with a tiny MLP which only forwards once per pixel. Instead of pre-training and baking a continuous NeRF into grids [19], we treat voxel values as parameters and directly optimize them like [15, 52]. Despite the “mip” name, Mip-VoG only trains one density voxel grid and one feature voxel grid that represent the high-resolution space. The lower resolution representations can then be inferred by downsampling the optimized grid progressively using low-pass filter and interpolation algorithms [13]. Given a single 3D point sampled from a camera ray, Mip-VoG first calculates the level of detail (LOD) via ray differentials [20], as a pixel-to-voxel ratio represents the point’s footprint on the full resolution voxel grids. Then the scene interests of that point is sampled by interpolating two neighboring level grids. The points of the camera ray casted from low resolution thus will be represented by a wider area in the space, resulting in large sample rate with more lower frequencies.

We evaluate our method on the widely studied NeRF datasets such as Synthetic-NeRF [33] and Multiscale-NeRF [3] following MipNeRF’s multi-scale setting [3]. The results show that, compared to state-of-the-art real-time techniques, our multiscale representation successfully tackled multi-resolution training and achieve higher accuracy in anti-aliasing rendering.

2. Related Works

Scene Representation for View Synthesis Various scene representations have been proposed for the task of view synthesis. Light field representation [11, 24, 25, 46] and Lumi-graph [17, 6] directly interpolate the input images, which must be dense to synthesize the novel views. To reduce the appetite of the dense capture, following works further represent the light field as a neural network [48, 2]. Layered depth images [12, 45, 47, 55] can alleviate the requirement of input denseness but depend on the accuracy of the depth maps to render photorealistic images. Recent researches propose to estimate the multiplane images (MPIs) [14, 27, 32, 51, 60, 68] for forward-facing scenes, and estimate the voxel grid [49, 29] to captures inward-facing scene. One popular category of view synthesis methods uses mesh-based representations [12, 45, 47, 55] which are naturally amenable to real-time rendering with highly optimized rasterization pipelines. Yet, these methods requires template meshes as a prior to overcome gradient-based optimization problem.

Recently, NeRF [33] emerges as a popular method for novel view synthesis. By using a MLP as an implicit and continuous volumetric representation, NeRF maps from a

3D coordinate to the volume density and view-dependent emission at that position. The success of NeRF brings numbers of attention into neural volumetric rendering for view synthesis. Many follow-on works have extended NeRF to generative models [7, 54, 44, 35], generalization [56, 64] dynamic scenes [37, 26, 40, 30, 43], relighting[4, 50, 67], and editing [38, 39, 53, 65, 28, 62], etc. Rendering an image from NeRF involves querying a large neural network at multiple 3D locations per pixel, yielding roughly a minute to render a single frame. To address the issue, some recent arts are proposed to improve the efficiency of NeRF’s neural volumetric rendering via leveraging explicit representation [8, 52, 15, 60] or decomposing the scene into sub-regions with smaller neural networks [42, 41].

Real-time Neural Rendering A series of works have been proposed to satisfy the real-time rendering requirement. PlenOctrees [63] presents a spherical harmonic representation of radiance and converts it into a PlenOctree data structure. FastNeRF [16] re-factorizes the NeRF and caches the scene of interest using a dense voxel grid for efficient rendering. Instant-NGP [34] uses a hash-table to store the feature vectors and fully-fuses CUDA kernels to accelerate rendering. SNeRG [19] proposes a deferred architecture and extracts the scene properties from a pre-trained model into a sparse grid data structure. MobileNeRF [9] represents the scene as a set of textured polygons and use polygon rasterization to render a image with features at every pixel, which are decoded by a small view-dependent MLP. Nevertheless, these explicit representations are not scale-agnostic, thus cannot be effectively learned from the training images with multiple resolutions. We primarily compare with SNeRG and MobileNeRF in our experiments since they have been shown to work on lower-powered devices without access to CUDA.

Reducing Aliasing in Rendering One straightforward solution to reduce aliasing for coordinate-based neural representations is supersampling [58], which requires casting multiple rays through pixel during rendering to get the final result. This is a powerful technique to weaken aliasing, but it aggravates the already slow rendering procedure of NeRF. Hence it can only be used in offline rendering. To improve the efficiency, Mip-NeRF [3] proposes to cast a conical frustum into the scene space and render the 3D region instead of a single point. To avoid heavy computation burden and approximate the 3D region rendering, their algorithm queries the network by IPE of the 3D input region to output the final density and radiance. Due to the heavy reliance on the network to decode the scale information, Mip-NeRF cannot leverage pre-cache techniques to enable real-time capability. Another common technique for reducing aliasing is pre-filtering [36, 21, 61, 5], which pre-filters the maps on

a coarse mesh *e.g.* color maps, normal maps, linearly and separately. This technique is affordable for real-time rendering since the computational cost has been moved to the time before rendering. One standard method used in many 3D rendering applications is mip mapping [13, 59, 10]. A serialization of images or textures, each of which is a progressively lower resolution representation of the previous one, are pre-computed ahead of time to increase rendering speed and reduce aliasing artifacts for real-time inference. Traditional mip mapping is performed on the texture mapping of 3D mesh, we extend this idea to 3D neural volumetric rendering and perform mipmapping on the voxel grids data structure instead of a map.

Relation to DVGO and Instant-NGP There are some remarkable concurrent works study the voxel representation for efficient rendering. Still, there are some difference between Mip-VoG and these works. DVGO [52] progressively optimize a higher resolution voxel grid in the training for finer details, but it does not consider a multi-scale representation. Besides, DVGO stores the implicit feature for radiance emission and predict the final pixel color by a shallow MLP. By contrast, our Mip-VoG stores the explicit value for diffuse color and implicit feature for view-dependent specular radiance. Instant-NGP [34] introduces a hash encoding approach based on a multi-resolution structure for speedy high-quality image synthesis. Their approach simultaneously trains several dense grid with different scales and concatenates the feature from each for further prediction. This representation only works for single-scale images since its scale-invariant. In contrast, our method only retains a single voxel grid during training and can adaptively sample from Mip-VoG with different LOD.

3. Method

3.1. Review of NeRF

NeRF [33] uses a MLP parameterized by θ as a continuous volumetric function to represent a scene. The network takes input as the view direction d and 3D coordinate $r(t)$ sampled from a camera ray $r(t) = o + td$, and predict the volume density σ at that 3D position together with the view-dependent radiance c from that view direction:

$$\sigma(t), c(t) = \text{MLP}_\theta(r(t), d). \quad (1)$$

A vital assumption made by NeRF is to model the density σ only depend on location, while emitted color is conditional on 3D coordinate $r(t)$ and view direction d . In the rendering procedure, NeRF takes the predicted densities and emissions $\{\sigma(t_i), c(t_i)\}_{i=1}^N$ along the ray casted from a pixel, and approximate a volume rendering integral [31] to derive

the final color of that pixel:

$$\hat{C}(r) = \sum_{i=1}^N T_i \left(1 - \exp(-\sigma(t_i)\delta(t_i)) \right) c(t_i), \quad (2)$$

$$\text{with } T_i = \exp\left(-\sum_{j=1}^{i-1} \sigma(t_j)\delta_j\right),$$

where $\delta(t_i) = t_{i+1} - t_i$ is the distance between adjacent samples. One can find that rendering a single ray for each pixel requires evaluating the MLP hundreds of times, resulting in significantly slow rendering speed.

3.2. Deferred NeRF

As discussed previously, real-time rendering can be achieved by pre-computing as many as scene properties. While the scene geometry (volume density) can be directly stored, NeRF relies on a continuous function to represent view-dependent effects. To address this problem, SNeRG [19] introduces a residual architecture that first caches the point-wise pre-trained volume density $\sigma(t)$, diffuse color $c_d(t)$ and 4-dimension feature vector $f_s(t)$. The pixel-wise diffuse color and feature vector are obtained through volume rendering (same as NeRF):

$$\hat{C}_d(r) = \sum_{i=1}^N T_i \left(1 - \exp(-\sigma(t_i)\delta(t_i)) \right) c_d(t_i), \quad (3)$$

$$F_s(r) = \sum_{i=1}^N T_i \left(1 - \exp(-\sigma(t_i)\delta(t_i)) \right) f_s(t_i). \quad (4)$$

Then, a tiny MLP parameterized by ϕ , which forwards once for each pixel based on the feature $F_s(r)$ and view direction d , is applied to predict the pixel-wise specular color as a view-dependent residual:

$$\hat{C}_s(r) = \text{MLP}_\phi(F_s(r), d). \quad (5)$$

The final color of the pixel is obtained by the summation of diffuse color and specular color:

$$\hat{C}(r) = \hat{C}_d(r) + \hat{C}_s(r). \quad (6)$$

Vanilla SNeRG involves pre-training a continuous representation first and caching voxel-wise σ , c_d and f_s into a sparse voxel grid. In contrast, our method directly learns an explicit representation from scratch, which can be directly used for efficient multiscale representation. We optimize $\sigma \in \mathbb{R}$ in one density Mip-VoG V_{den} and $c_d \in \mathbb{R}^3$ together with $f_s \in \mathbb{R}^4$ in one color Mip-VoG V_{rgb} . The overview of our framework is shown in Fig. 1. In the following section, we present the query algorithms of Mip-VoG.

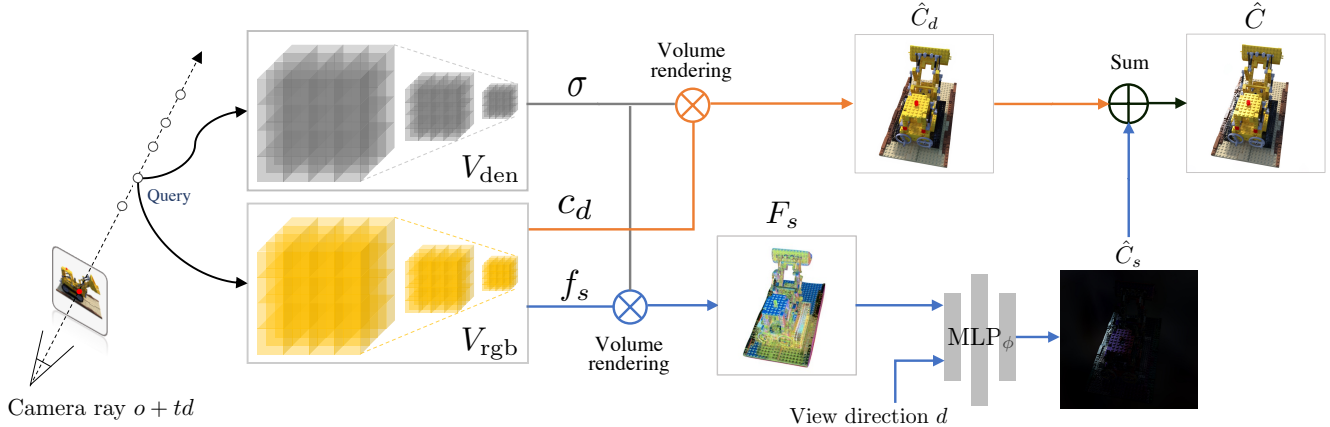


Figure 1: **Rendering framework overview.** We based our pipeline design on deferred NeRF [19] with explicit training of Mip-VoG. Given a point sampled from a camera ray, we query the density Mip-VoG and color Mip-VoG to predict the 1D volume density, 3D diffuse color and 4D feature-vector. We then aggregate the diffuse colors and feature vectors along the ray through volume rendering integral. After that, a tiny MLP is used to predict a pixel-wise view-dependent specular color residual by using the accumulated feature-vector together with the view direction. The final color prediction is the summation of diffuse color and specular color.

3.3. Mip Voxel Grids

Mip-VoG uses multiple downsampled “much in little” voxel grids for querying the scene interest of a 3D location. To sample from a Mip-VoG for a single 3D point in the space, one needs to first calculate the LOD, as a “correct” scale with respect to the full resolution voxel grids. Filtering and downsampling operation are then applied on the full resolution voxel grids to derive voxel grids with lower scale progressively. The sampled value from the Mip-VoG with the correspondence of the LOD is derived via interpolation between two different scales of voxel grids with neighbor level. For simplicity, we drop the subscript of V_{den} and V_{rgb} , using a single notation $V^{(0)}$ indicates the original voxel grids at level 0. By analogy, $V^{(1)}, V^{(2)}, V^{(k)}$ denote the downsampled voxel grids at level 1, level 2 and level k .

3.3.1 Level of Detail

Given a single ray cast through a pixel, ray differentials represent a pair of differentially offset rays slightly above or to the right of the original ray [20, 1]. We extend this idea to the volumetric rendering with voxel grids. Denote u, v, w as the unit coordinates as regard to the voxel space $V^{(0)}$, for a pixel of the frame with image space coordinates x and y , the ray differentials are defined as derivatives of the ray with respect to image space coordinates:

$$\frac{\partial V^{(0)}}{\partial x} = \left\langle \frac{\partial u}{\partial x} \frac{\partial v}{\partial x} \frac{\partial w}{\partial x} \right\rangle, \quad \frac{\partial V^{(0)}}{\partial y} = \left\langle \frac{\partial u}{\partial y} \frac{\partial v}{\partial y} \frac{\partial w}{\partial y} \right\rangle. \quad (7)$$

By applying a first-order Taylor approximation, we can get an expression for the extent of a pixel’s footprint in voxel

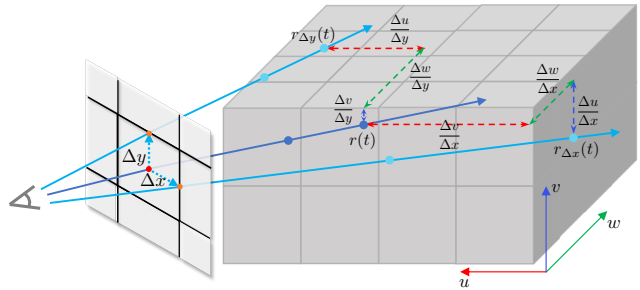


Figure 2: **Ray differentials.** To calculate the LOD of a point on the camera ray, we first cast two differentiated rays generated by adding offset as the half pixel size on x and y axis on the screen space. Then for each point on the original ray, we compute the point’s unit distance to its neighbours along three axis on the full-resolution voxel grids. The LOD is calculated based on the largest length of the texel-to-pixel ratio.

space based on the pixel-to-voxel spacing:

$$\frac{\partial V^{(0)}}{\partial x} \approx \left\langle \frac{\Delta u}{\Delta x} \frac{\Delta v}{\Delta x} \frac{\Delta w}{\Delta x} \right\rangle, \quad \frac{\partial V^{(0)}}{\partial y} \approx \left\langle \frac{\Delta u}{\Delta y} \frac{\Delta v}{\Delta y} \frac{\Delta w}{\Delta y} \right\rangle. \quad (8)$$

Intuitively, this can be seen as the per-axis offset on the voxel grids made by the deviation of the ray in the image plane. As illustrated in Fig. 2, we adopt $\Delta x, \Delta y$ as the half pixel size along the x and y axis of the image plane, since it can approximate the footprint of a pixel. Given the position of a point $r(t)$ and its neighbors $r_{\Delta x}(t), r_{\Delta y}(t)$ in the world space, the offset in voxel unit coordinate can be derived by

the ratio between the distance per axis and the voxel size:

$$\Delta u = \frac{T_u}{V_u}, \Delta v = \frac{T_v}{V_v}, \Delta w = \frac{T_w}{V_w}, \quad (9)$$

where T_u, T_v, T_w are the distance to the neighbors in the world space and V_u, V_v, V_w are voxel size on u, v, w along three axes. Then following the convention of mipmapping [18, 59], the LOD λ can be calculated as¹:

$$\lambda = 1/3 * \log_2(\rho)$$

with $\rho = \max \left(\sqrt{\left(\frac{\Delta u}{\Delta x}\right)^2 + \left(\frac{\Delta v}{\Delta x}\right)^2 + \left(\frac{\Delta w}{\Delta x}\right)^2}, \right.$ (10)

$$\left. \sqrt{\left(\frac{\Delta u}{\Delta y}\right)^2 + \left(\frac{\Delta v}{\Delta y}\right)^2 + \left(\frac{\Delta w}{\Delta y}\right)^2} \right).$$

3.3.2 Filtering and Sampling

After obtaining the LOD λ , one needs to sample the interests from the voxel grid with the corresponding scale. To achieve Mip-VoG, we progressively down-sample the original voxel grid $V^{(0)}$ to a lower resolution. Before downsampling, a low-pass filter γ is applied to filter high-frequency information. Following most common mipmap techniques [23], for every one level up (integer) in λ , by default we do downsampling operation with a scale of 1/2 to get a new voxel grid:

$$V^{(k+1)} = \Downarrow_{1/2} (\gamma(V^{(k)})), \quad (11)$$

where $\Downarrow_{1/2} (\cdot)$ represents the downsampling with 1/2 resolution. We use linear interpolation as the down-sample filtering. For instance, given the dimension of $V^{(0)}$ is $D \times N_x \times N_y \times N_z$, $V^{(1)}$ will be scaled to $D \times N_x/2 \times N_y/2 \times N_z/2$, where D is the dimension of modality. By analogy, we can get a feature voxel grid with higher LOD and lower resolution, as shown in Fig. 3.

In order to match the continuity of non-integer LOD λ , we use quadrilinear interpolation to aggregate the sample from two voxel grids with neighbouring (upper and lower) levels. Let $f(V, p)$ denote the sampling function of the voxel grids, and $\mu \in \{\sigma, c_d, f_s\}$ represent the stores value, the interpolation process can be formulated as:

$$\mu = (\lceil \lambda \rceil - \lambda) f(V^{(\lceil \lambda \rceil)}, r(t)) + (\lambda - \lfloor \lambda \rfloor) f(V^{(\lfloor \lambda \rfloor)}, r(t)), \quad (12)$$

where $\lfloor \cdot \rfloor$ and $\lceil \cdot \rceil$ are the floor and ceiling function.

3.3.3 Optimization

Similar to the prior work [52], our optimization is mainly divided into two stages: coarse and fine. In the coarse

¹Since the number of voxels drops by 8x each level, we have $\log_8(\rho) = \log_2(\rho) / \log_2(8) = 1/3 * \log_2(\rho)$.

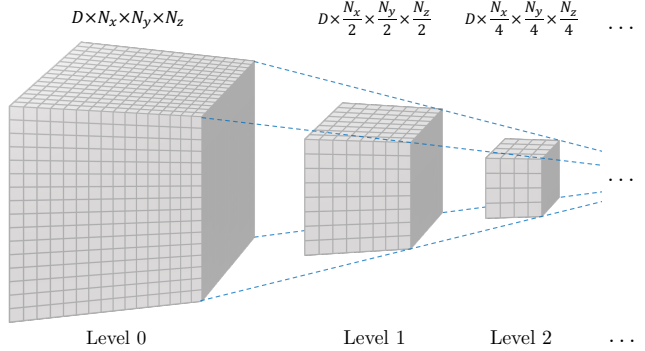


Figure 3: **Mip-VoG structure.** For each level up of LOD, we first perform filtering on the previous voxel grids using low-pass filter, and then downsample it to half resolution by linear interpolation. The query value for a 3D point is sampled by interpolating the results from two neighbor voxel grids according to point’s LOD.

stage, we normally train $V_{\text{den}(c)} \in \mathbb{R}^{1 \times N_x^{(c)} \times N_y^{(c)} \times N_z^{(c)}}$ with $V_{\text{rgb}(c)} \in \mathbb{R}^{3 \times N_x^{(c)} \times N_y^{(c)} \times N_z^{(c)}}$ without using Mip-VoG, as to only obtain a rough 3D geometry $V_{\text{den}(c)}$ for reducing the number of sampling points in the fine stage. In the fine stage, we train a density Mip-VoG $V_{\text{den}(f)} \in \mathbb{R}^{1 \times N_x^{(f)} \times N_y^{(f)} \times N_z^{(f)}}$ and a color Mip-VoG $V_{\text{rgb}(f)} \in \mathbb{R}^{7 \times N_x^{(f)} \times N_y^{(f)} \times N_z^{(f)}}$ with a tiny MLP $_{\phi}$ as introduced before. We use gradient-descent to directly optimize value in voxel grids. As the gradient of the linear interpolation used in Mip-VoG downsampling $\Downarrow_{1/2}$ is tractable, the gradient from voxel grids with different resolution can be naturally aggregated and propagated. The loss function is the square error between the predicted pixel color and the ground truth:

$$\mathcal{L}_r = \sum_i \|C(r_i) - \hat{C}(r_i)\|_2^2. \quad (13)$$

4. Experiments

In light of our previous discussion, we primarily compare the results under the real-time rendering setting. We mainly evaluate our method on a simple multiscale synthetic dataset from Mip-NeRF [3] designed to better validate the accuracy on multi-resolution scenes. We also conduct the experiment on its single-resolution version blender dataset introduced in the original NeRF paper [33], in order to probe our aliasing performance of the model training on a single-scale dataset. We report the commonly studied three error metrics: PSNR, SSIM [57], and LPIPS [66], and show some qualitative results.

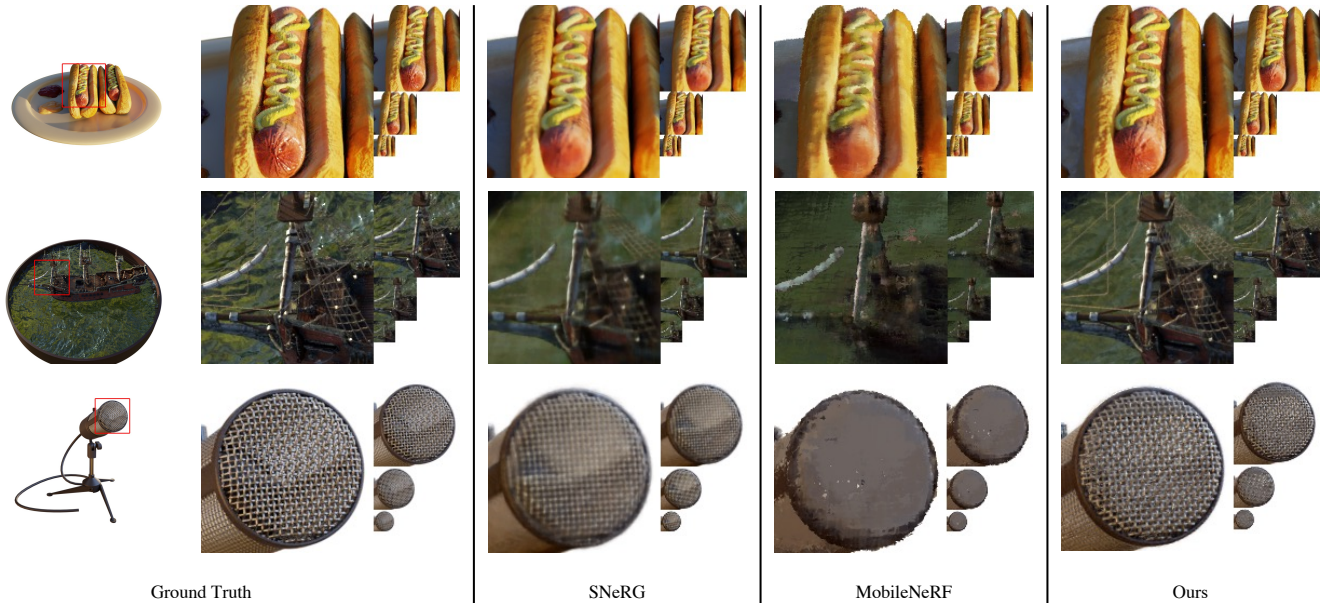


Figure 4: **Multiscale-NeRF**. We demonstrate Mip-VoG rendering results compared to other baselines on the test set from three scenes, trained and evaluated on multiscale dataset. We visualize a crop region (shown in red box) on a same image at 4 different scales as an image pyramid. MobileNeRF yields over smooth results on all scales, while SNeRG lost high frequencies in high-resolution images and product aliasing in low-resolution frames. Our method surpass the baselines by a large margin as the rendering quality is significantly better.

Method	PSNR \uparrow				SSIM \uparrow				LPIPS \downarrow			
	Full Res	1/2 Res	1/4 Res	1/8 Res	Full Res	1/2 Res	1/4 Res	1/8 Res	Full Res	1/2 Res	1/4 Res	1/8 Res
SNeRG [19]	27.043	28.405	30.044	28.544	0.912	0.932	0.952	0.950	0.100	0.067	0.047	0.049
MobileNeRF [9]	24.115	25.127	26.633	27.930	0.868	0.885	0.913	0.938	0.141	0.112	0.078	0.050
MobileNeRF [9] w/o SS	23.730	24.425	25.308	25.364	0.861	0.875	0.898	0.910	0.149	0.128	0.104	0.091
Ours	30.333	31.290	31.055	29.014	0.946	0.956	0.960	0.955	0.069	0.049	0.045	0.048

Table 2: **Multiscale-NeRF**. For quantitative comparison of models trained and evaluated on multiscale dataset. All the metrics of the scale are averaged across eight scenes. “w/o SS” removes supersampling from MobileNeRF [9].

4.1. Datasets

1. Synthetic-NeRF [33] presented in the original NeRF paper contains eight scenes. In this single-scale dataset, each scene consists 100 training images and 200 test images with uniform $800 * 800$ resolution. The model trained on this dataset can learn all the high-frequency details from the full resolution images, without being harmed by training images at multiple scale.
2. Multiscale-NeRF [3] is a straightforward conversion to Synthetic-NeRF [33] for analyzing multiscale training and aliasing. It was generated by taking each image in Synthetic-NeRF and box downsampling it by a factor of 2, 4, and 8 (and modifying the camera intrinsics accordingly). The three downscaled images along with the original images are then combined into one single dataset. Hence this dataset contains image with four different scales for both training and test set, and

the size has been quadrupled. The average evaluation metric is reported as the arithmetic mean of each error metric across all four scales. As suggested by Mip-NeRF [3], we adopt the Area Loss for all the methods which scale the pixel’s loss by the footprint size in the full resolution images, to balance the influence between high and low resolution pixels.

4.2. Implementation Details

In our experiments, we set the same hyperparameters for single-scale and multiscale datasets. In the coarse stage, the resolution of the voxel grid for both density and color is $(128 \times 128 \times 128)$, while in the fine stage, it raises to $(512 \times 512 \times 512)$. The low pass filter is adopted as the Mean Filter with kernel size 5. We use “shifted softplus” mentioned in Mip-NeRF [3] as the density activation. The initial values of alpha is 10^{-6} in the coarse training stage, and 10^{-2} in the fine training stage. Our tiny MLP follows

the architecture used in SNERG [19]. We use the Adam optimizer [22] to train both voxels and the deferred MLP, the learning rate are set to $4 * 10^{-3}$ for the deferred MLP and $1 * 10^{-1}$ for the voxel grids. In addition, we train 10k and 20k iterations for the coarse phase and fine phase with the batch size of 8192, respectively. For real-time web renderer, we convert Mip-VoG to the sparse voxel grid data structure [19] and implement our query procedure in WebGL using the THREE.js library to increase the rendering speed. In terms of a fair comparison, all the methods are trained on a 80GB A100 GPU and tested on laptop GPU. We report the rendering speed and storage in Tab. 3.

Method	Storage(MB) ↓	FPS(Dev1) ↑	FPS(Dev2) ↑
SNeRG	87	121	197
MobileNeRF	126	125	356
Ours	62	53	71

Table 3: **Disk storage in MB and rendering speed in frames per second (FPS)**. Dev1: Lenovo Legion 7 (laptop) w/ NVIDIA RTX 2070 SUPER; Dev2: Alienware M15R6 (laptop) w/ NVIDIA RTX 3080.

4.3. Results

Multiscale-NeRF The performance of Mip-VoG for this dataset can be seen in Tab. 2. As shown in the table, our method outperforms baselines on all metrics across all scales. While the result is a consequence multi-scale training and anti-aliasing, since this dataset contains different resolution images for both training and test set. We defer the ablation into the following parts. Here we visualize some qualitative results in Fig 4. One can see that other real-time rendering approaches produce blurry results on high resolution images, due to the challenging issue of multi-scale training. In contrast, our result learns high-frequency information in the full resolution images and output low-frequencies in low resolution images. We visualize the computed LOD in Fig. 5, the pixel-wise results is accumulated through the ray through volume rendering integral.

Synthetic-NeRF Since the baselines models are not compatible with multiscale training, we eliminate the factor of non-uniform training images but to examine the effectiveness on anti-aliasing rendering. For this dataset the model is trained on single scale images and evaluated on the multi-scale version, since the testset Multiscale-NeRF contains all the test images in Synthetic-NeRF. This inference scenario can be seen as rendering the single scale dataset but with the distance to the viewpoint has increased by scale factors of 2, 4, and 8 (also known as minification). In Tab. 4, excluding the effect of multiscale training set, our method is still outperforming the baselines on all metrics on high-resolution

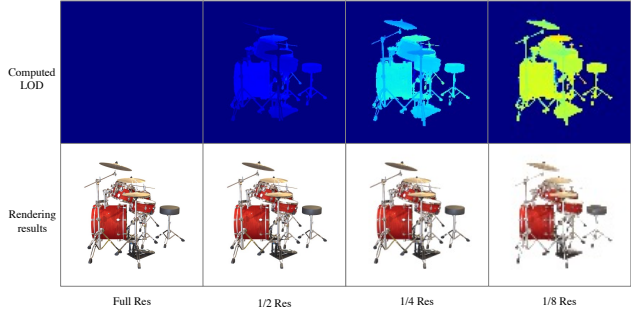


Figure 5: **Visualization of LOD**. We visualize the per-pixel LOD at four different scales. The value is computed using volume rendering integral of the points’ LOD along the ray. We scaled the low-resolution rendered images to the size of full resolution for better visibility and comparison. Brighter color indicates higher values.

images, with a smaller model storage (Tab. 3). MobileNeRF [9] can perform better results on low-resolution images, thanks to the strategy of supersampling. While removing this technique from it in the inference phase, our method outperforms the baseline models across all the scales. Interestingly, MobileNeRF can learn well in single-scale training and afford supersampling in real-time rendering, it suffers a lot from training with multiple resolution images as we find in the previous results. We shown some inference results in Fig. 6. One can find our method produce more low-frequency details to ground truth in the low-resolution images if zooming in, while in high-resolution images our method preserve sharp high-frequency details. This results verify that our method effectively learns a multiscale representation since it improves the both multi-resolution training and anti-aliasing.

4.4. Ablations

In this section we mainly analysis the effectiveness of the contribution of Mip-VoG to the model, and give some insights into the filtering algorithm. We perform all the experiments on Multiscale-NeRF [3], and report the average PSNR over the eight scenes.

Mipmapping To better examine the validness of Mip-VoG, we ablate this technique from training and testing respectively. While produce the rendering result without Mip-VoG reflects the ability of training with the images at multiple resolution, removing it from training effectively shows the improvement on anti-aliasing. As the results shown in Tab. 5, training without Mip-VoG shows lower accuracy in high-resolution test images and higher quality in low-resolution frames. This result is consistent with the studies in Mip-NeRF [3], as the area loss would force model to

Method	PSNR \uparrow				SSIM \uparrow				LPIPS \downarrow			
	Full Res	1/2 Res	1/4 Res	1/8 Res	Full Res	1/2 Res	1/4 Res	1/8 Res	Full Res	1/2 Res	1/4 Res	1/8 Res
SNERG [19]	29.333	30.065	28.355	25.373	0.940	0.949	0.946	0.924	0.134	0.091	0.097	0.144
MobileNeRF [9]	29.448	30.654	31.144	30.000	0.934	0.947	0.957	0.959	0.077	0.054	0.042	0.037
MobileNeRF [9] w/o SS	28.290	28.447	27.317	25.212	0.926	0.935	0.935	0.917	0.093	0.077	0.079	0.094
Ours	30.355	30.467	28.766	26.566	0.949	0.956	0.951	0.935	0.062	0.050	0.058	0.073

Table 4: **Synthetic-NeRF**. Performance of models that trained on single scale Synthetic-NeRF but evaluated on Multiscale-NeRF. All the metrics of the scale are averaged across eight scenes. “w/o SS” removes supersampling from MobileNeRF [9].

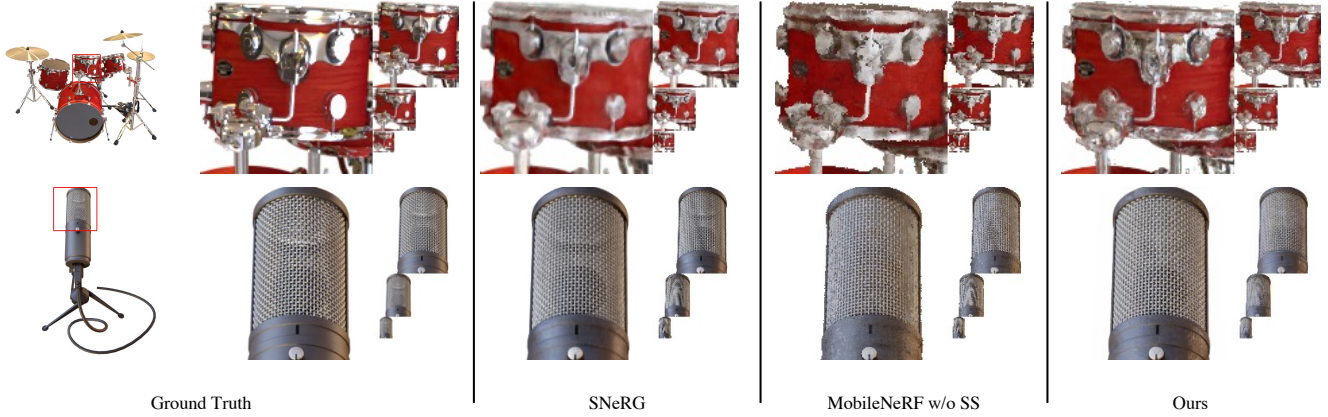


Figure 6: **Synthetic-NeRF**. We demonstrate Mip-VoG rendering results compared to other baselines on the test set from two scenes, trained on single-scale dataset. We visualize a crop region (shown in red box) on a same image at 4 different scales as an image pyramid. Our method outputs the sharp details on high-resolution images and smooth results on low-resolution images, with regards to the ground truth.

“overfit” on low-resolution training samples. While training with mip-VoG can help preserve high-frequencies rendering without Mip-VoG would produce aliasing in low-resolution frames, as the metrics of ‘Ours w/o te-mip’ in lower scale is worse than the baseline. Hence, using Mip-VoG in both training and testing contributes the multiscale training and anti-aliasing rendering.

Method	PSNR \uparrow			
	Full Res	1/2 Res	1/4 Res	1/8 Res
Ours w/o tr-mip te-mip	29.690	30.897	30.201	27.371
Ours w/o tr-mip	29.631	30.217	29.461	27.663
Ours w/o te-mip	30.348	31.146	29.581	26.669
Ours	30.333	31.290	31.055	29.014

Table 5: **Mipmapping ablation**. We conduct the experiments on the Multiscale-NeRF with respectively dropping the Mip-VoG in training and testing, denoted as “tr-mip” and “te-mip” in the table.

Low-pass Filter One design in the sampling phase is that the voxel grids are pre-filtered by a low-pass filter, which can preserve the high frequency information in the training and abandon them in rendering. We test our model based

on three type of filters: no filter, gaussian filter and mean filter. We also experiment the filter with different kernel size. The results are shown in Tab. 6. Firstly, using filter yields a better performance on the rendering quality across all the scales. Secondly, Mip-VoG is robust to different filter while the superior performance is achieved when the mean filter with kernel size 5 is chosen. Finally, using too small or too large kernel size tends to slightly harm the filtering outcome, as size 5 surpass the other two for both mean filter and gaussian filter.

Filter	PSNR \uparrow			
	Full Res	1/2 Res	1/4 Res	1/8 Res
None	29.995	31.043	30.718	28.534
Mean (size 3)	30.211	31.179	30.997	29.005
Mean (size 5)	30.333	31.290	31.055	29.014
Mean (size 7)	30.210	31.177	30.995	29.002
Gaussian (size 3)	30.011	31.068	30.733	28.575
Gaussian (size 5)	30.052	31.078	30.759	28.683
Gaussian (size 7)	30.005	31.059	30.731	28.505

Table 6: **Low-pass filter ablation**. We demonstrate the sensitivity of the low-pass filter with respective to the filter type and the kernel size.

5. Conclusion

In the paper, we have presented a multiscale representation for real-time anti-aliasing rendering method. We base our work on the voxel grids representation with a deferred architecture of NeRF. We proposed to use mip voxel grids, which yields the point-wise sampling from the voxel grids of different scales according to the level of detail computed by ray differentials. To generate multiple levels of Mip-VoG, we leverage the low-pass filter and interpolation filtering to downsample the original full resolution voxel grid progressively. The final scene properties of a 3D is sampled from two neighbor voxel grids using quadrilinear interpolation. Experiments show our method effectively learns a multiscale representation from the training images and provides higher accuracy in real-time anti-aliasing rendering. Our main bottleneck of rendering speed is the computation burden of ray differentials which requires tracking two neighbor rays on the screen space. We sacrifice the speed of original SNeRG formulation to provide a multiscale representation. We hope our approach will be valuable to future research on multiscale training and real-time anti-aliasing rendering for neural rendering models.

References

- [1] Tomas Akenine-Möller, Jim Nilsson, Magnus Andersson, Colin Barré-Brisebois, Robert Toth, and Tero Karras. Texture level of detail strategies for real-time ray tracing. In *Ray Tracing Gems*, pages 321–345. Springer, 2019.
- [2] Benjamin Attal, Jia-Bin Huang, Michael Zollhöfer, Johannes Kopf, and Changil Kim. Learning neural light fields with ray-space embedding. In *Proceedings of the IEEE/CVF Conference on Computer Vision and Pattern Recognition*, pages 19819–19829, 2022.
- [3] Jonathan T Barron, Ben Mildenhall, Matthew Tancik, Peter Hedman, Ricardo Martin-Brualla, and Pratul P Srinivasan. Mip-nerf: A multiscale representation for anti-aliasing neural radiance fields. In *Proceedings of the IEEE/CVF International Conference on Computer Vision*, pages 5855–5864, 2021.
- [4] Sai Bi, Zexiang Xu, Pratul Srinivasan, Ben Mildenhall, Kalyan Sunkavalli, Miloš Hašan, Yannick Hold-Geoffroy, David Kriegman, and Ravi Ramamoorthi. Neural reflectance fields for appearance acquisition. *arXiv preprint arXiv:2008.03824*, 2020.
- [5] Eric Bruneton and Fabrice Neyret. A survey of nonlinear pre-filtering methods for efficient and accurate surface shading. *IEEE Transactions on Visualization and Computer Graphics*, 18(2):242–260, 2011.
- [6] Chris Buehler, Michael Bosse, Leonard McMillan, Steven Gortler, and Michael Cohen. Unstructured lumigraph rendering. In *Proceedings of the 28th annual conference on Computer graphics and interactive techniques*, pages 425–432, 2001.
- [7] Eric R Chan, Marco Monteiro, Petr Kellnhofer, Jiajun Wu, and Gordon Wetzstein. pi-gan: Periodic implicit generative adversarial networks for 3d-aware image synthesis. In *Proceedings of the IEEE/CVF conference on computer vision and pattern recognition*, pages 5799–5809, 2021.
- [8] Anpei Chen, Zexiang Xu, Andreas Geiger, Jingyi Yu, and Hao Su. Tensorf: Tensorial radiance fields. *arXiv preprint arXiv:2203.09517*, 2022.
- [9] Zhiqin Chen, Thomas Funkhouser, Peter Hedman, and Andrea Tagliasacchi. Mobilenerf: Exploiting the polygon rasterization pipeline for efficient neural field rendering on mobile architectures. *arXiv preprint arXiv:2208.00277*, 2022.
- [10] Cyril Crassin, Fabrice Neyret, Sylvain Lefebvre, Miguel Sainz, and Elmar Eisemann. Beyond triangles: gigavoxels effects in video games. In *SIGGRAPH 2009: Talks*, page 78. ACM, 2009.
- [11] Abe Davis, Marc Levoy, and Fredo Durand. Unstructured light fields. In *Computer Graphics Forum*, volume 31, pages 305–314. Wiley Online Library, 2012.
- [12] Helisa Dharmo, Keisuke Tateno, Iro Laina, Nassir Navab, and Federico Tombari. Peeking behind objects: Layered depth prediction from a single image. *Pattern Recognition Letters*, 125:333–340, 2019.
- [13] Jon P Ewins, Marcus D Waller, Martin White, and Paul F Lister. Mip-map level selection for texture mapping. *IEEE Transactions on Visualization and Computer Graphics*, 4(4):317–329, 1998.
- [14] John Flynn, Michael Broxton, Paul Debevec, Matthew DuVall, Graham Fyffe, Ryan Overbeck, Noah Snavely, and Richard Tucker. Deepview: View synthesis with learned gradient descent. In *Proceedings of the IEEE/CVF Conference on Computer Vision and Pattern Recognition*, pages 2367–2376, 2019.
- [15] Sara Fridovich-Keil, Alex Yu, Matthew Tancik, Qinhong Chen, Benjamin Recht, and Angjoo Kanazawa. Plenoxels: Radiance fields without neural networks. In *Proceedings of the IEEE/CVF Conference on Computer Vision and Pattern Recognition*, pages 5501–5510, 2022.
- [16] Stephan J Garbin, Marek Kowalski, Matthew Johnson, Jamie Shotton, and Julien Valentin. Fastnerf: High-fidelity neural rendering at 200fps. In *Proceedings of the IEEE/CVF International Conference on Computer Vision*, pages 14346–14355, 2021.
- [17] Steven J Gortler, Radek Grzeszczuk, Richard Szeliski, and Michael F Cohen. The lumigraph. In *Proceedings of the 23rd annual conference on Computer graphics and interactive techniques*, pages 43–54, 1996.
- [18] Paul S Heckbert et al. Texture mapping polygons in perspective. Technical report, Citeseer, 1983.
- [19] Peter Hedman, Pratul P Srinivasan, Ben Mildenhall, Jonathan T Barron, and Paul Debevec. Baking neural radiance fields for real-time view synthesis. In *Proceedings of the IEEE/CVF International Conference on Computer Vision*, pages 5875–5884, 2021.
- [20] Homan Igehy. Tracing ray differentials. In *Proceedings of the 26th annual conference on Computer graphics and interactive techniques*, pages 179–186, 1999.
- [21] Anton S Kaplanyan, Stephan Hill, Anjul Patney, and Aaron E Lefohn. Filtering distributions of normals for shading anti-aliasing. In *High Performance Graphics*, pages 151–162, 2016.
- [22] Diederik P Kingma and Jimmy Ba. Adam: A method for stochastic optimization. *arXiv preprint arXiv:1412.6980*, 2014.
- [23] Sylvain Lefebvre and Hugues Hoppe. Parallel controllable texture synthesis. In *ACM SIGGRAPH 2005 Papers*, pages 777–786. 2005.
- [24] Anat Levin and Fredo Durand. Linear view synthesis using a dimensionality gap light field prior. In *2010 IEEE Computer Society Conference on Computer Vision and Pattern Recognition*, pages 1831–1838. IEEE, 2010.
- [25] Marc Levoy and Pat Hanrahan. Light field rendering. In *Proceedings of the 23rd annual conference on Computer graphics and interactive techniques*, pages 31–42, 1996.
- [26] Zhengqi Li, Simon Niklaus, Noah Snavely, and Oliver Wang. Neural scene flow fields for space-time view synthesis of dynamic scenes. In *Proceedings of the IEEE/CVF Conference on Computer Vision and Pattern Recognition*, pages 6498–6508, 2021.
- [27] Zhengqi Li, Wenqi Xian, Abe Davis, and Noah Snavely. Crowdsampling the plenoptic function. In *European Conference on Computer Vision*, pages 178–196. Springer, 2020.
- [28] Steven Liu, Xiuming Zhang, Zhoutong Zhang, Richard Zhang, Jun-Yan Zhu, and Bryan Russell. Editing conditional

- radiances fields. In *Proceedings of the IEEE/CVF International Conference on Computer Vision*, pages 5773–5783, 2021.
- [29] Stephen Lombardi, Tomas Simon, Jason Saragih, Gabriel Schwartz, Andreas Lehrmann, and Yaser Sheikh. Neural volumes: Learning dynamic renderable volumes from images. *arXiv preprint arXiv:1906.07751*, 2019.
- [30] Ricardo Martin-Brualla, Noha Radwan, Mehdi SM Sajjadi, Jonathan T Barron, Alexey Dosovitskiy, and Daniel Duckworth. Nerf in the wild: Neural radiance fields for unconstrained photo collections. In *Proceedings of the IEEE/CVF Conference on Computer Vision and Pattern Recognition*, pages 7210–7219, 2021.
- [31] Nelson Max. Optical models for direct volume rendering. *IEEE Transactions on Visualization and Computer Graphics*, 1(2):99–108, 1995.
- [32] Ben Mildenhall, Pratul P Srinivasan, Rodrigo Ortiz-Cayon, Nima Khademi Kalantari, Ravi Ramamoorthi, Ren Ng, and Abhishek Kar. Local light field fusion: Practical view synthesis with prescriptive sampling guidelines. *ACM Transactions on Graphics (TOG)*, 38(4):1–14, 2019.
- [33] Ben Mildenhall, Pratul P Srinivasan, Matthew Tancik, Jonathan T Barron, Ravi Ramamoorthi, and Ren Ng. Nerf: Representing scenes as neural radiance fields for view synthesis. *Communications of the ACM*, 65(1):99–106, 2021.
- [34] Thomas Müller, Alex Evans, Christoph Schied, and Alexander Keller. Instant neural graphics primitives with a multiresolution hash encoding. *arXiv preprint arXiv:2201.05989*, 2022.
- [35] Michael Niemeyer and Andreas Geiger. Giraffe: Representing scenes as compositional generative neural feature fields. In *Proceedings of the IEEE/CVF Conference on Computer Vision and Pattern Recognition*, pages 11453–11464, 2021.
- [36] Marc Olano and Dan Baker. Lean mapping. In *Proceedings of the 2010 ACM SIGGRAPH symposium on Interactive 3D Graphics and Games*, pages 181–188, 2010.
- [37] Julian Ost, Fahim Mannan, Nils Thuerey, Julian Knodt, and Felix Heide. Neural scene graphs for dynamic scenes. In *Proceedings of the IEEE/CVF Conference on Computer Vision and Pattern Recognition*, pages 2856–2865, 2021.
- [38] Keunhong Park, Utkarsh Sinha, Jonathan T Barron, Sofien Bouaziz, Dan B Goldman, Steven M Seitz, and Ricardo Martin-Brualla. Nerfies: Deformable neural radiance fields. In *Proceedings of the IEEE/CVF International Conference on Computer Vision*, pages 5865–5874, 2021.
- [39] Keunhong Park, Utkarsh Sinha, Peter Hedman, Jonathan T Barron, Sofien Bouaziz, Dan B Goldman, Ricardo Martin-Brualla, and Steven M Seitz. Hypernerf: A higher-dimensional representation for topologically varying neural radiance fields. *arXiv preprint arXiv:2106.13228*, 2021.
- [40] Albert Pumarola, Enric Corona, Gerard Pons-Moll, and Francesc Moreno-Noguer. D-nerf: Neural radiance fields for dynamic scenes. In *Proceedings of the IEEE/CVF Conference on Computer Vision and Pattern Recognition*, pages 10318–10327, 2021.
- [41] Daniel Rebain, Wei Jiang, Soroosh Yazdani, Ke Li, Kwang Moo Yi, and Andrea Tagliasacchi. Derf: Decomposed radiance fields. In *Proceedings of the IEEE/CVF Conference on Computer Vision and Pattern Recognition*, pages 14153–14161, 2021.
- [42] Christian Reiser, Songyou Peng, Yiyi Liao, and Andreas Geiger. Kilonerf: Speeding up neural radiance fields with thousands of tiny mlps. In *Proceedings of the IEEE/CVF International Conference on Computer Vision*, pages 14335–14345, 2021.
- [43] Viktor Rudnev, Mohamed Elgharib, William Smith, Lingjie Liu, Vladislav Golyanik, and Christian Theobalt. Nerf for outdoor scene relighting. In *Computer Vision—ECCV 2022: 17th European Conference, Tel Aviv, Israel, October 23–27, 2022, Proceedings, Part XVI*, pages 615–631. Springer, 2022.
- [44] Katja Schwarz, Yiyi Liao, Michael Niemeyer, and Andreas Geiger. Graf: Generative radiance fields for 3d-aware image synthesis. *Advances in Neural Information Processing Systems*, 33:20154–20166, 2020.
- [45] Jonathan Shade, Steven Gortler, Li-wei He, and Richard Szeliski. Layered depth images. In *Proceedings of the 25th annual conference on Computer graphics and interactive techniques*, pages 231–242, 1998.
- [46] Lixin Shi, Haitham Hassanieh, Abe Davis, Dina Katabi, and Fredo Durand. Light field reconstruction using sparsity in the continuous fourier domain. *ACM Transactions on Graphics (TOG)*, 34(1):1–13, 2014.
- [47] Meng-Li Shih, Shih-Yang Su, Johannes Kopf, and Jia-Bin Huang. 3d photography using context-aware layered depth inpainting. In *Proceedings of the IEEE/CVF Conference on Computer Vision and Pattern Recognition*, pages 8028–8038, 2020.
- [48] Vincent Sitzmann, Semon Rezkikov, Bill Freeman, Josh Tenenbaum, and Fredo Durand. Light field networks: Neural scene representations with single-evaluation rendering. *Advances in Neural Information Processing Systems*, 34:19313–19325, 2021.
- [49] Vincent Sitzmann, Justus Thies, Felix Heide, Matthias Nießner, Gordon Wetzstein, and Michael Zollhofer. Deepvoxels: Learning persistent 3d feature embeddings. In *Proceedings of the IEEE/CVF Conference on Computer Vision and Pattern Recognition*, pages 2437–2446, 2019.
- [50] Pratul P Srinivasan, Boyang Deng, Xiuming Zhang, Matthew Tancik, Ben Mildenhall, and Jonathan T Barron. Nerv: Neural reflectance and visibility fields for relighting and view synthesis. In *Proceedings of the IEEE/CVF Conference on Computer Vision and Pattern Recognition*, pages 7495–7504, 2021.
- [51] Pratul P Srinivasan, Richard Tucker, Jonathan T Barron, Ravi Ramamoorthi, Ren Ng, and Noah Snavely. Pushing the boundaries of view extrapolation with multiplane images. In *Proceedings of the IEEE/CVF Conference on Computer Vision and Pattern Recognition*, pages 175–184, 2019.
- [52] Cheng Sun, Min Sun, and Hwann-Tzong Chen. Direct voxel grid optimization: Super-fast convergence for radiance fields reconstruction. In *Proceedings of the IEEE/CVF Conference on Computer Vision and Pattern Recognition*, pages 5459–5469, 2022.

- [53] Edgar Tretschk, Ayush Tewari, Vladislav Golyanik, Michael Zollhöfer, Christoph Lassner, and Christian Theobalt. Non-rigid neural radiance fields: Reconstruction and novel view synthesis of a dynamic scene from monocular video. In *Proceedings of the IEEE/CVF International Conference on Computer Vision*, pages 12959–12970, 2021.
- [54] Alex Trevithick and Bo Yang. Grf: Learning a general radiance field for 3d representation and rendering. In *Proceedings of the IEEE/CVF International Conference on Computer Vision*, pages 15182–15192, 2021.
- [55] Shubham Tulsiani, Richard Tucker, and Noah Snavely. Layer-structured 3d scene inference via view synthesis. In *Proceedings of the European Conference on Computer Vision (ECCV)*, pages 302–317, 2018.
- [56] Qianqian Wang, Zhicheng Wang, Kyle Genova, Pratul P Srinivasan, Howard Zhou, Jonathan T Barron, Ricardo Martin-Brualla, Noah Snavely, and Thomas Funkhouser. Ibrnet: Learning multi-view image-based rendering. In *Proceedings of the IEEE/CVF Conference on Computer Vision and Pattern Recognition*, pages 4690–4699, 2021.
- [57] Zhou Wang, Alan C Bovik, Hamid R Sheikh, and Eero P Simoncelli. Image quality assessment: from error visibility to structural similarity. *IEEE transactions on image processing*, 13(4):600–612, 2004.
- [58] Turner Whitted. An improved illumination model for shaded display. In *ACM Siggraph 2005 Courses*, pages 4–es. 2005.
- [59] Lance Williams. Pyramidal parametrics. In *Proceedings of the 10th annual conference on Computer graphics and interactive techniques*, pages 1–11, 1983.
- [60] Suttisak Wizadwongsa, Pakkapon Phongthawee, Jiraphon Yenphraphai, and Supasorn Suwajanakorn. Nex: Real-time view synthesis with neural basis expansion. In *Proceedings of the IEEE/CVF Conference on Computer Vision and Pattern Recognition*, pages 8534–8543, 2021.
- [61] Lifan Wu, Shuang Zhao, Ling-Qi Yan, and Ravi Ramamoorthi. Accurate appearance preserving prefiltering for rendering displacement-mapped surfaces. *ACM Transactions on Graphics (TOG)*, 38(4):1–14, 2019.
- [62] Bangbang Yang, Chong Bao, Junyi Zeng, Hujun Bao, Yinda Zhang, Zhaopeng Cui, and Guofeng Zhang. Neumesh: Learning disentangled neural mesh-based implicit field for geometry and texture editing. In *Computer Vision–ECCV 2022: 17th European Conference, Tel Aviv, Israel, October 23–27, 2022, Proceedings, Part XVI*, pages 597–614. Springer, 2022.
- [63] Alex Yu, Ruilong Li, Matthew Tancik, Hao Li, Ren Ng, and Angjoo Kanazawa. Plenotrees for real-time rendering of neural radiance fields. In *Proceedings of the IEEE/CVF International Conference on Computer Vision*, pages 5752–5761, 2021.
- [64] Alex Yu, Vickie Ye, Matthew Tancik, and Angjoo Kanazawa. pixelnerf: Neural radiance fields from one or few images. In *Proceedings of the IEEE/CVF Conference on Computer Vision and Pattern Recognition*, pages 4578–4587, 2021.
- [65] Yu-Jie Yuan, Yang-Tian Sun, Yu-Kun Lai, Yuewen Ma, Rongfei Jia, and Lin Gao. Nerf-editing: geometry editing of neural radiance fields. In *Proceedings of the IEEE/CVF Conference on Computer Vision and Pattern Recognition*, pages 18353–18364, 2022.
- [66] Richard Zhang, Phillip Isola, Alexei A Efros, Eli Shechtman, and Oliver Wang. The unreasonable effectiveness of deep features as a perceptual metric. In *Proceedings of the IEEE conference on computer vision and pattern recognition*, pages 586–595, 2018.
- [67] Xiuming Zhang, Pratul P Srinivasan, Boyang Deng, Paul Debevec, William T Freeman, and Jonathan T Barron. Nerfactor: Neural factorization of shape and reflectance under an unknown illumination. *ACM Transactions on Graphics (TOG)*, 40(6):1–18, 2021.
- [68] Tinghui Zhou, Richard Tucker, John Flynn, Graham Fyffe, and Noah Snavely. Stereo magnification: Learning view synthesis using multiplane images. *arXiv preprint arXiv:1805.09817*, 2018.